Inorganic Chemistry

Article

Cite This: *Inorg. Chem.* XXXX, XXX, XXX−XXX

pubs.acs.org/IC

# Complex Cation and Spin Orders in the High-Pressure Ferrite $CoFe_3O_5$

Ka H. Hong,[†] Elena Solana-Madruga,[†] Mauro Coduri,[‡] and J. Paul Attfield*,[†]

[†]Centre for Science at Extreme Conditions and School of Chemistry, University of Edinburgh, West Mains Road, Edinburgh EH9 3FD, United Kingdom

[‡]European Synchrotron Radiation Facility, 71 avenue des Martyrs, Grenoble 38000, France

*Supporting Information*

**ABSTRACT:** A ferrite in the $Sr_2Tl_2O_5$-type $MFe_3O_5$ family with M = Co has been synthesized at 12 GPa pressure. Neutron diffraction shows the sample to be Co deficient with composition $Co_{0.6}Fe_{3.4}O_5$. The Co/Fe cation distribution is found to be profoundly different from those of $MFe_3O_5$ analogs and lies between normal and inverse limits, as $Co^{2+}$ substitutes across trigonal prismatic and one of the two octahedral sites. $CoFe_3O_5$ shows complex magnetic behavior with weak ferromagnetism below $T_{C1} \approx 300$ K and a second transition to ferrimagnetic order at $T_{C2} \approx 100$ K. Spin scattering of carriers leads a substantial increase in the hopping activation energy below $T_{C1}$, and a small negative magnetoresistance is observed at low temperatures.

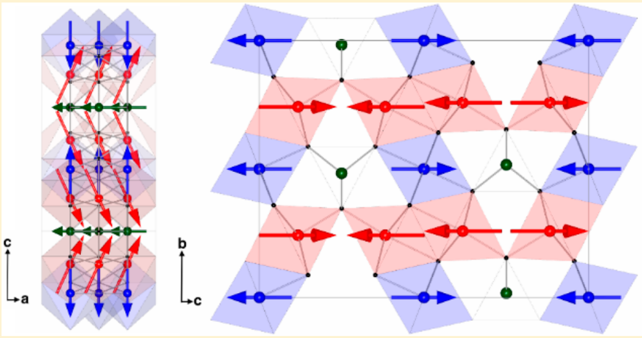

## INTRODUCTION

Iron oxide spinels and related magnetic materials are important for many applications and also for fundamental interest in couplings between spin, charge, orbital, and lattice degrees of freedom. Magnetite, $Fe_3O_4$, has been studied intensively since 1939 when Verwey reported a metal−insulator transition accompanied by a structural distortion.[1] The low-temperature structure has a complex charge and orbital ordering that leads to the formation of trimerons−linear orbital molecule clusters of three Fe ions.[2] Further notable magnetic and electronic orders have subsequently been discovered in the underexplored $Fe_nO_{n+1}$ and substituted $MFe_{n-1}O_{n+1}$ homologous series. The $n = 4$ phase $Fe_4O_5$, prepared using high-pressure high-temperature (HPHT) synthesis,[3] has an incommensurate charge order at 150 K below which dimeron and trimeron-like groups of Fe ions are formed,[4] and higher $Fe_nO_{n+1}$ homologues with $n > 4$ have also been made at pressure.[5] Studies of $n = 6$ $CaFe_5O_7$ have revealed a coupled structural and magnetic transition at 360 K accompanied by charge ordering.[6−8]

In addition to $Fe_4O_5$, other $n = 4$ $MFe_3O_5$ phases have also been found to have notable properties. $CaFe_3O_5$, which was first reported in 1980 and can be prepared at ambient pressure,[9] has recently been shown to have long-range electronic phase separation. Magnetic ordering below 302 K leads to segregation into $Fe^{2+}/Fe^{3+}$ charge averaged and charge ordered phases with formation of trimerons in the latter.[10] $MnFe_3O_5$, discovered under HPHT conditions, shows a rich variety of magnetic ordered states on cooling below $T_N = 350$ K, and $Fe^{2+}/Fe^{3+}$ charge ordering at 60 K leads to spin reorientation.[11,12] $MgFe_3O_5$ was also reported in a study of the $Fe_4O_5$-$Mg_2Fe_2O_5$ solid solution, but the crystal structure and magnetic properties were not reported.[13]

The $MFe_3O_5$ phases adopt the orthorhombic $Sr_2Tl_2O_5$-type structure with space group *Cmcm*.[14] This has three independent cation sites M1, M2, and M3 in a 2:1:1 ratio, where M1 and M2 form edge-sharing $MO_6$ octahedra channeled by triangular prisms containing the M3 site, as shown in Figure 1. The M3 site is occupied by large $M^{2+}$ = Ca, Mn, and Fe cations in the above $MFe_3O_5$ materials. However, it is unclear whether transition metals smaller than iron will also occupy trigonal prismatic M3 sites or will prefer octahedral M1 and M2. These alternative distributions are analogous to the much-studied normal and inverse cation arrangements in spinels. Hence we report here the HPHT synthesis of $CoFe_3O_5$, the crystal structure including the cation distribution, and the electrical and magnetic properties.

## EXPERIMENTAL SECTION

**HPHT Synthesis.** CoO and $Fe_3O_4$ powders were ground together in a 1:1 ratio and were heated under pressure at 1200 °C in a Pt capsule for 20 min in a two-stage Walker-type module. Reaction at 10 GPa pressure was unsuccessful, but 12 GPa gave a polycrystalline product of apparent composition $CoFe_3O_5$. Several batches of material were synthesized under the latter conditions.

**Magnetic and Electrical Property Measurements.** A Quantum Design MPMS XL SQUID magnetometer was used to carry out magnetization measurements. Electrical resistivity measurements were carried out with a Quantum Design PPMS.

**Received:** August 30, 2018

DOI: 10.1021/acs.inorgchem.8b02458
*Inorg. Chem.* XXXX, XXX, XXX−XXX

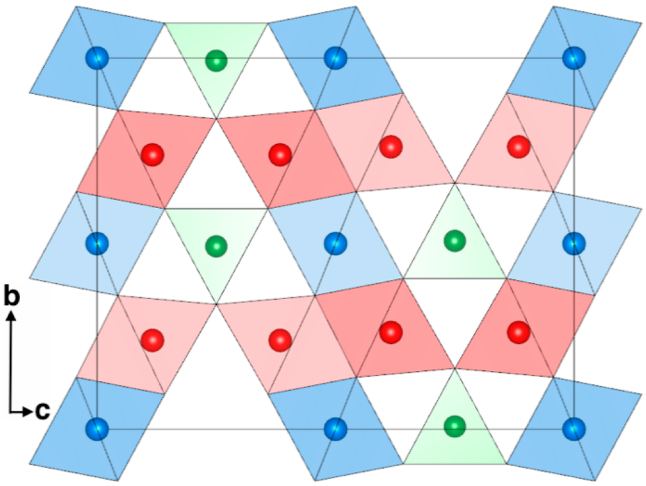

**Figure 1.** Polyhedral projection of the *Cmcm* structure of $CoFe_3O_5$ at 300 K with M1 site octahedra shown in red, M2 octahedra in blue, and M3 triangular prisms in green. Oxygens are located at the corners of polyhedra.

**Crystal and Magnetic Structures.** HPHT reaction products were initially characterized by powder X-ray diffraction collected with a Bruker D2 diffractometer using Cu $K_\alpha$ radiation. High-resolution powder synchrotron X-ray diffraction (PSXRD) data were collected at the ID22 beamline of the ESRF with incident wavelength 0.39994 Å. A glass capillary with an outer diameter of 0.3 mm was used to contain the polycrystalline sample of approximately 8 mg. Low-temperature diffraction data were collected from 5 to 90 K using a liquid helium cryostat system and from 90 to 400 K with an Oxford Cryosystems nitrogen cryostream. High-resolution time-of-flight powder neutron diffraction (PND) data were collected at the WISH beamline of the ISIS facility, with 50 mg of powder from several high-pressure syntheses packed into a vanadium can. Diffraction patterns were collected between 10 and 400 K using a closed cycle refrigerator (CCR) with a hot stage. The crystal and magnetic structures of $CoFe_3O_5$ were Rietveld-fitted using the FullProf Suite and General Structure Analysis System (GSAS),[15,16] and images were generated using VESTA.[17]

## ■ RESULTS AND DISCUSSION

**Synthesis.** Phase formation was confirmed using laboratory powder X-ray diffraction. A Rietveld fit to the diffraction pattern (Figure S1) confirms an orthorhombic *Cmcm* phase isostructural with the $MFe_3O_5$ (M = Ca, Fe, and Mn) analogs. The room-temperature lattice parameters of $CoFe_3O_5$ are $a$ = 2.8982(4), $b$ = 9.767(2), and $c$ = 12.567(1) Å, with a cell volume of $V$ = 355.7(1) Å$^3$. Further structural results are described later.

**Magnetic and Electrical Properties.** Magnetic susceptibilities in Figure 2a reveal two magnetic transitions for $CoFe_3O_5$. A small magnetic upturn is observed at $T_{C1} \approx 300$ K, and a second transition is seen at $T_{C2} \approx 100$ K. Both are accompanied by divergence of zero-field cooled (ZFC) and field cooled (FC) measurements indicating ferromagnetic contributions. Magnetization-field loops, shown in the inset of Figure 2a, show a small remnant magnetization of $M_r = 0.014$ $\mu_B$ per formula unit at 350 K, mostly likely due to traces of ferromagnetic spinel impurities. $M_r$ increases to 0.06 $\mu_B$ on cooling from 350 to 200 K through $T_{C1}$, revealing an intrinsic weak ferromagnetism, and increases further on cooling through $T_{C2}$ to 0.75 $\mu_B$ at 4 K, consistent with a ferrimagnetic order. Two similar magnetic transitions were reported for $MnFe_3O_5$ at 350 and 60 K.[12]

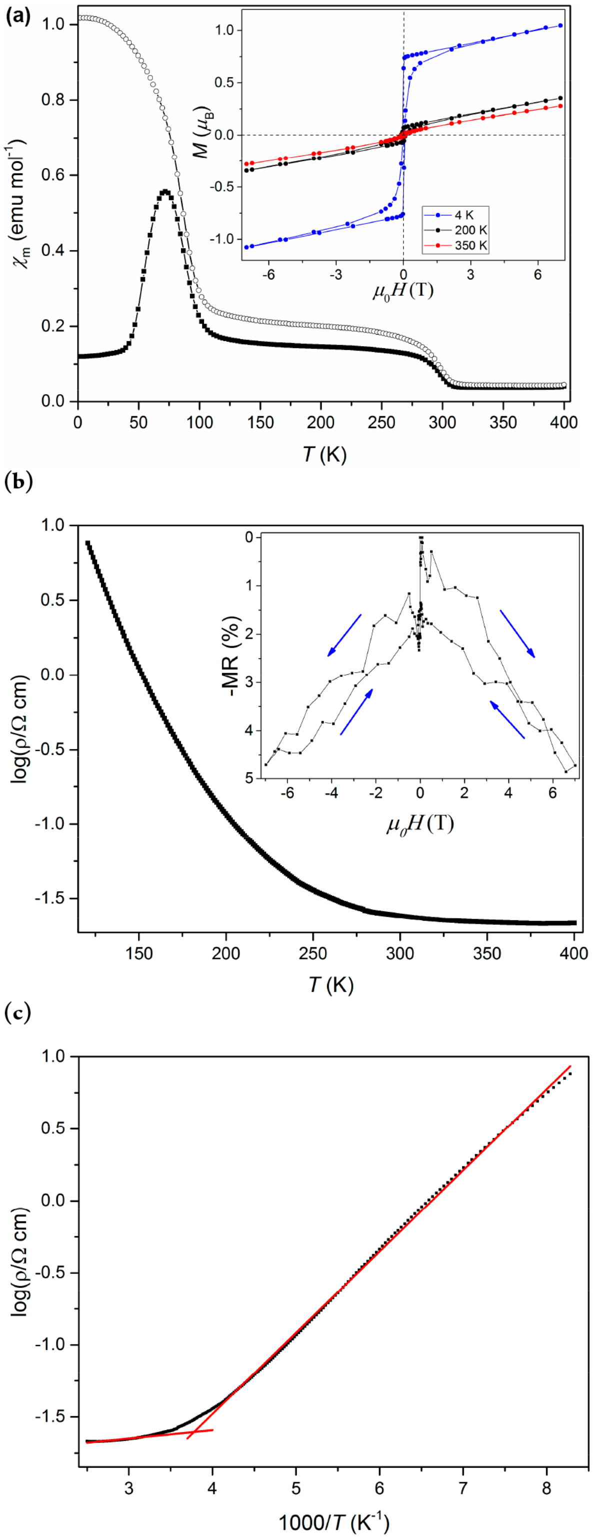

**Figure 2.** (a) ZFC (closed symbols) and FC (open symbols) magnetic susceptibilities for $CoFe_3O_5$ in a 0.2 T field. Inset shows magnetization-field loops at 4, 200, and 350 K. (b) $Log_{10}$ of the electrical resistivity against temperature. Inset shows magnetoresistance at 125 K. (c) $Log_{10}$(resistivity)−reciprocal temperature plot showing Arrhenius fits above and below $T_{C1} \approx 300$ K.

The electrical resistivity of a polycrystalline pellet of $CoFe_3O_5$ shows semiconducting behavior (Figure 2b), and the resistance was too great to be measured below 120 K. The

DOI: 10.1021/acs.inorgchem.8b02458
*Inorg. Chem.* XXXX, XXX, XXX−XXX

high-temperature activation energy for electron hopping, fitted as an Arrhenius $\rho = A\exp(E_a/k_BT)$ dependence in Figure 2c, is $E_a$ = 14 meV showing that the material behaves as a highly doped semiconductor. The slope deviates on cooling below $T_{C1} \approx 300$ K ($1000/T_{C1} \approx 3.3$), and the 130−245 K region has a substantially higher $E_a$ = 112 meV revealing a strong antiferromagnetic spin scattering contribution. A small magnetoresistance effect of $MR = -5\%$ in a 7 T field at 125 K is observed, as shown in the inset to Figure 2b, consistent with partial suppression of the spin scattering term. $CoFe_3O_5$ has a larger $-MR$ than $CaFe_3O_5$ due to a higher magnetization at low temperature.

**Crystal Structure Determination.** The high contrast between the neutron scattering lengths of Fe and Co (9.45 and 2.49 fm respectively) enabled occupancies of the three cation sites to be determined from refinement against the high-resolution neutron diffraction data obtained at 400 K (Figure S2). This reveals that the M1 site is occupied exclusively by Fe, while the M2 and M3 sites contain Fe/Co mixtures as shown in Table 1. The overall refined composition of $Co_{0.58}Fe_{3.42}O_5$ is Co deficient. Refined amounts and compositions of CoO rock salt and $CoFe_2O_4$ spinel-type secondary phases were 11.2(7)% $Co_{0.86}Fe_{0.14}O$ and 3.2(1)% $Co_{0.95}Fe_{2.05}O_4$, showing that these impurities are relatively Co rich. Further details are in Table S1. M−O bond distances and derived values for the bond valence sum (BVS), estimated by a standard interpolation method,[18,19] are shown in Table 2.

Table 1. Lattice Parameters, Atomic Coordinates, Site Occupancies, and Isotropic Thermal Displacements from Neutron Refinements in *Cmcm* Space Group of $CoFe_3O_5$ at 400 K (Upper Values) and 10 K (Lower Values)[a]

| *a* (Å) | *b* (Å) | *c* (Å) | volume (Å$^3$) |
|---|---|---|---|
| 2.9048(2) | 9.7865(8) | 12.5884(6) | 357.86(4) |
| 2.8836(1) | 9.7968(3) | 12.5385(5) | 354.21(2) |

| atom | *x* | *y* | *z* | Occ[b] Fe/Co | $B_{iso}$ (Å$^2$) |
|---|---|---|---|---|---|
| M1 | 1/2 | 0.2438(6) | 0.1166(3) | 1/0 | 2.0(1) |
| | | 0.2419(5) | 0.1176(3) | | 1.4(1) |
| M2 | 0 | 0 | 0 | 0.78(1)/0.22 | 2.0 |
| | | | | | 1.4 |
| M3 | 0 | 0.4792(8) | 1/4 | 0.64(1)/0.36 | 2.0 |
| | | 0.4834(8) | | | 1.4 |
| O1 | 1/2 | 0.3437(11) | 1/4 | 1 | 0.9(1) |
| | | 0.3460(11) | | | 0.8(1) |
| O2 | 0 | 0.3569(7) | 0.0447(6) | 1 | 0.9 |
| | | 0.3587(7) | 0.0431(6) | | 0.8 |
| O3 | 0 | 0.0902(8) | 0.1449(6) | 1 | 0.9 |
| | | 0.0872(8) | 0.1478(6) | | 0.8 |

[a] Estimated standard deviations in independent variables are shown in parentheses. $\chi^2$ = 13.1 and 11.8, $R_{wp}$ = 10.7 and 8.7%, and $R_p$ = 12.9 and 10.1% at 400 and 10 K, respectively. [b] Variable occupancies were refined against 400 K neutron data and were fixed in lower temperature refinements.

Table 2. Metal−Oxygen Bond Lengths with Derived Mean values ⟨ ⟩ and BVSs Shown for $CoFe_3O_5$ at 400 K (Upper Values) and 10 K (Lower Values)

| bond | distance (Å) | bond | distance (Å) |
|---|---|---|---|
| M1−O1 | 1.943(7) | M2−O2 (×4) | 2.095(6) |
| | 1.948(7) | | 2.071(5) |
| M1−O2 | 2.257(9) | M2−O3 (×2) | 2.026(8) |
| | 2.243(9) | | 2.040(8) |
| M1−O2 (×2) | 2.038(7) | ⟨M2−O⟩ | 2.072(3) |
| | 2.064(7) | | 2.061(3) |
| M1−O3 (×2) | 2.120(8) | BVS(M2) | 2.4(1) |
| | 2.127(7) | | 2.3(1) |
| ⟨M1−O⟩ | 2.086(3) | M3−O1 (×2) | 1.967(9) |
| | 2.096(3) | | 1.973(10) |
| BVS(M1) | 2.4(1) | M3−O3 (×4) | 2.245(7) |
| | 2.5(1) | | 2.180(7) |
| | | ⟨M3−O⟩ | 2.152(3) |
| | | | 2.111(3) |
| | | BVS(M3) | 2.0(1) |
| | | | 2.2(1) |

The long average M3−O distance and the M3 BVS show that this trigonal prismatic site is occupied by divalent cations, in keeping with other $Sr_2Tl_2O_5$-type materials, while the similar average distances and BVSs for the octahedral M1 and M2 sites indicate that they have a mix of divalent and trivalent cations. The estimated bond valence sums (BVSs) of the three cation sites in $CoFe_3O_5$ are similar to those of $Fe_4O_5$ at room temperature. The site-specific composition, written as $(M3)(M1)_2(M2)O_5$ for comparison with the standard $MFe_3O_5$ formula, is thus $(Co^{2+}_{0.36}Fe^{2+}_{0.64})(Fe^{2+}_{0.33}Fe^{3+}_{0.67})_2(Co^{2+}_{0.22}Fe^{2+}_{0.11}Fe^{3+}_{0.67})O_5$ assuming that Fe is oxidized to the trivalent state in preference to Co. The cation distribution reveals that this Co-deficient sample lies between the postulated normal and inverse $MFe_3O_5$ distributions with around 60% of the substituted $Co^{2+}$ at the trigonal prismatic sites (normal distribution) and the remaining 40% at the octahedral sites (inverse distribution).

A surprisingly strong preference for Co to substitute for Fe at the octahedral M2 but not the M1 site is also discovered in $CoFe_3O_5$. The M1 site is found to have a higher BVS than M2 in other $MFe_3O_5$ materials, and a complete $Fe^{3+}/Fe^{2+}$ charge ordering over M1/M2 sites is observed in one phase of $CaFe_3O_5$.[10] Hence the tendency for cobalt to substitute as $Co^{2+}$ rather than $Co^{3+}$ probably drives the M2 octahedral site preference, although the disorder within our Co-deficient sample does not lead to a significant difference between the M1 and M2 site BVSs.

**Temperature Evolution of Crystal Structure.** The thermal evolution of the crystal structure of $CoFe_3O_5$ between 5 and 400 K has been studied using high-resolution PSXRD (Figure 3) and PND experiments. Rietveld fits showed that the orthorhombic *Cmcm* structure is adopted throughout this temperature range. Anisotropic thermal expansion of the lattice parameters is observed when cooled below $T_{C1} \approx 300$ K (Figures 4 and S3), with *a* and *c* contracting with decreasing temperature, while *b* expands. Another anomaly in the slope of the lattice parameters and cell volume is found at $T_{C2} \approx 100$ K. These observations show that the changes in magnetic order are coupled to the lattice leading to magnetostrictive effects.

Refined coordinates do not reveal any large changes in the crystal structure between 10 and 400 K. BVS's shown in Figure 5 remain approximately constant on cooling, although slight anomalies are seen around $T_{C2} \approx 100$ K accompanied by an increase in the tetragonal Jahn−Teller distortion parameter $Q_{JT}$ at site M1. The latter is consistent with intersite charge transfer increasing the $Fe^{3+}/Fe^{2+}$ ratio, as $Fe^{3+}$ has intrinsic $Q_{JT} = 0$, while orbitally degenerate $Fe^{2+}$ has negative $Q_{JT}$. Hence there are traces of the charge ordering seen in other $MFe_3O_5$

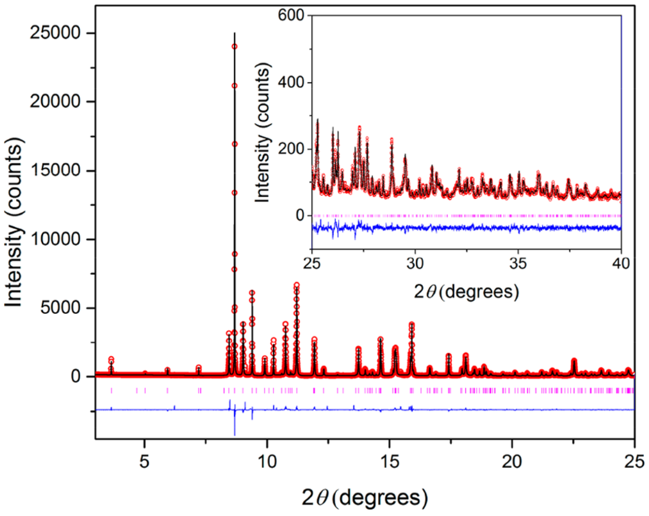

**Figure 3.** Rietveld fit to synchrotron powder diffraction profiles for $CoFe_3O_5$ at 300 K, with inset showing high-angle fitting ($\chi^2 = 8.5$, $R_{wp} = 12.3\%$ and $R_p = 9.4\%$).

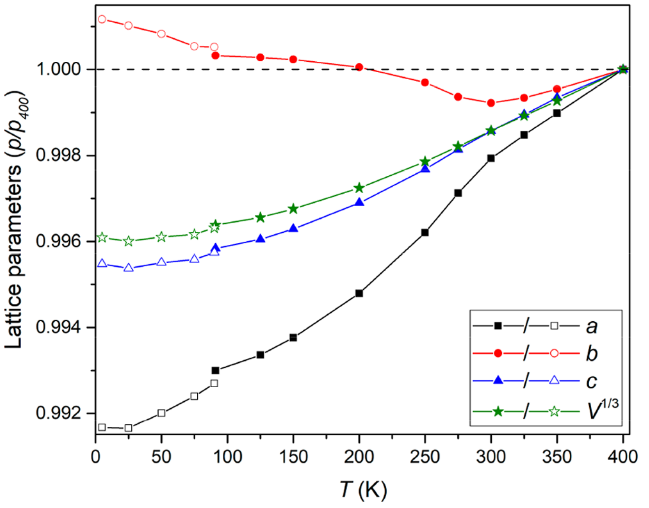

**Figure 4.** Changes in the lattice parameters relative to 400 K values obtained from PSXRD ($a_{400\ K} = 2.90423(3)$, $b_{400\ K} = 9.77325(8)$, and $c_{400\ K} = 12.5817(1)$ Å). Open/closed points were collected using helium cryostat/nitrogen cryostream systems.

materials, but the cation disorder in $CoFe_3O_5$ suppresses any clear charge and orbital ordering.

**Magnetic Structures.** High-resolution PND patterns collected at 10, 50, 150, and 400 K and additional short scans at intermediate temperatures were used to determine the magnetic structures of $CoFe_3O_5$ and to study their thermal evolution. Plots in Figure 6a reveal the appearance of magnetic reflections when $CoFe_3O_5$ is cooled below $T_{C1} \approx 300$ K, and additional magnetic peaks are observed below $T_{C2} \approx 100$ K. All of the magnetic reflections in both regimes were indexed by propagation vector [0 0 0], and analysis of the resulting irreducible representations for the spin order is shown in Table S2 with refined moment components in Table S3. The refined magnetic structures gave good fits to the data, as shown in Figure 6b. The magnetic contribution of the rock salt $Co_{0.86}Fe_{0.14}O$ phase, where spins order antiferromagnetically below ~300 K with a propagation vector of [1/2 1/2 1/2], was also included in the refinements.

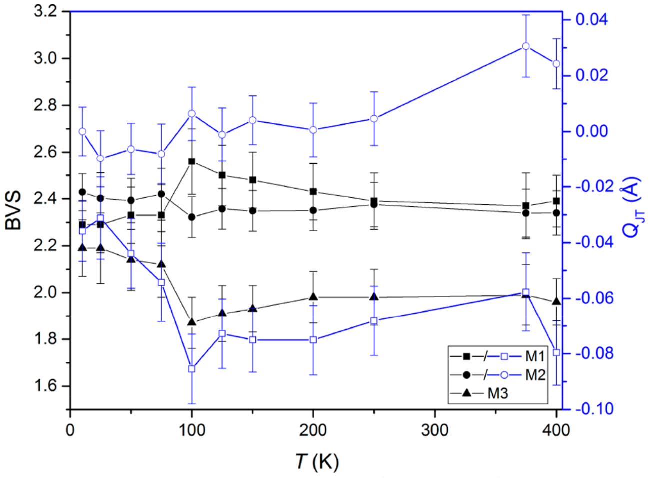

**Figure 5.** Temperature evolution of BVS (black points) and the tetragonal Jahn–Teller distortion parameter $Q_{JT}$ (blue points) for the octahedral cation sites in $CoFe_3O_5$, obtained from PND data.

The magnetic structures adopted by $CoFe_3O_5$ below $T_{C1}$ and $T_{C2}$ are presented in Figure 7a,b, respectively, and the thermal evolutions of the ordered moments are shown in Figure 7c. On cooling below $T_{C1} \approx 300$ K, the spins at the octahedral M1 and M2 sites order antiferromagnetically parallel to the *c* axis, while the M3 spins remain disordered. Canting of the spins toward the *b*-axis is allowed by symmetry, although the ordered component is too small to refine, and this weak ferromagnetism is the likely cause of the small net magnetization observed at 200 K in Figure 2a. The additional magnetic reflections below $T_{C2} \approx 100$ K are fitted by a ferromagnetic order of the M3 spins along the *a*-axis with canting of the M1 spins so that they gain a ferromagnetic *x*-component antiparallel to the M3 spins. Further low-temperature spin reorientations reported in $Fe_4O_5$ and $MnFe_3O_5$ are driven by $Fe^{2+}/Fe^{3+}$charge ordering. However, cation disorder in $CoFe_3O_5$ suppresses any charge ordering, and hence no further spin canting is observed at lower temperatures. The total ordered M1 moment at 10 K of 4.3 $\mu_B$ is consistent with near-$Fe^{3+}$spins, while smaller M2 and M3 moments of 3.3 and 2.6 $\mu_B$ reflect the Fe/Co disorder. The predicted net ferrimagnetic moment of 1.1 $\mu_B$ per formula unit at 10 K is comparable to the remnant magnetization of 0.75 $\mu_B$ observed at 2 K (Figure 2a).

The antiferromagnetic spin ordering of $CoFe_3O_5$ formed below $T_{C1}$ is the same as those reported in $MnFe_3O_5$ and in the charge averaged phase of $CaFe_3O_5$.[10,12] This is favored by dominant antiferromagnetic M1–M2 interactions through direct exchange and M–O–M superexchange between edge and corner sharing $M1O_6$ and $M2O_6$ octahedra. Weaker antisymmetric Dzyaloshinskii–Moriya (DM) interactions lead to canting and the observed weak ferromagnetism. Spins at the trigonal prismatic M3 sites are coupled to equal numbers of antiparallel M1 and M2 moments through M–O–M bridges, and so their long-range order is frustrated. Weaker DM interactions thus result in ferromagnetic order of M3 moments, perpendicular to the antiferromagnetic spins, below $T_{C2}$. Symmetric superexchange interactions between M3 and M1 spins lead to a canting of the latter such that they gain ferromagnetic components aligned antiparallel to the M3 spins. A similar coupled order of M3 and antiparallel M1 spin components is observed in the intermediate temperature spin

DOI: 10.1021/acs.inorgchem.8b02458
*Inorg. Chem.* XXXX, XXX, XXX−XXX

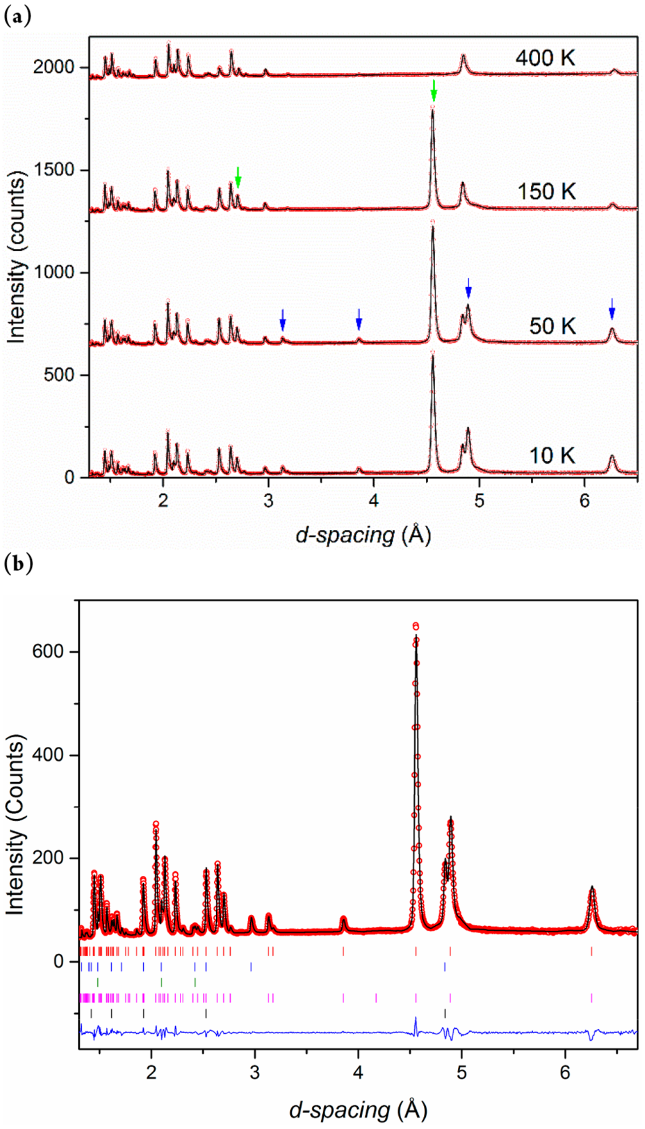

**Figure 6.** (a) Temperature evolution of the neutron diffraction pattern of $CoFe_3O_5$. Magnetic peak contributions indicated by green arrows in the 150 K pattern are (021) and (111), and those indicated by blue arrows at 50 K are (002), (020), (022), and (004), in order of descending *d*-spacing. Rietveld fits to the profiles are shown. (b) Full Rietveld plot for the 10 K data. Markers from top to bottom, respectively, show reflections from nuclear $CoFe_3O_5$, $CoFe_2O_4$, and CoO and magnetic $CoFe_3O_5$ and CoO type phases ($\chi^2$ = 12.5, $R_{wp}$ = 9.2% and $R_p$ = 10.1%).

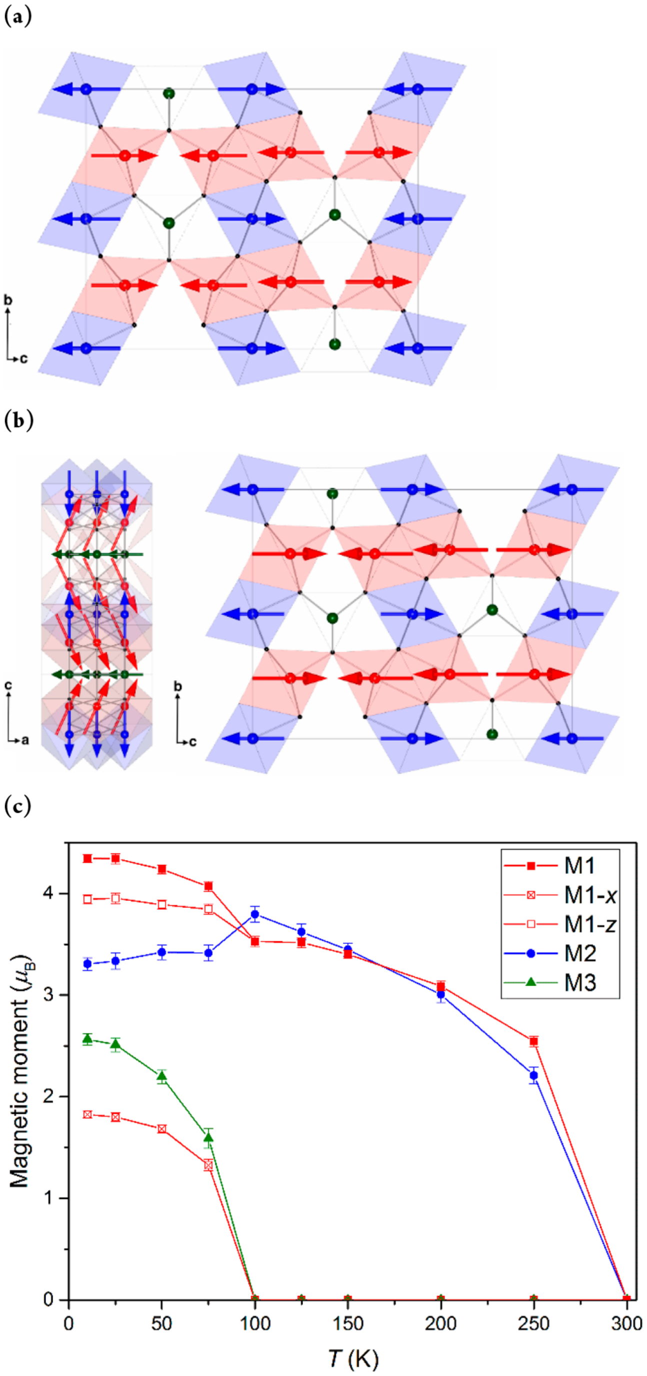

**Figure 7.** Magnetic structures of $CoFe_3O_5$ at (a) 150 and (b) 10 K. Octahedral M1 and M2 and trigonal prismatic M3 sites and moments are shown as red, blue, and green, respectively. (c) The temperature evolution of the ordered magnetic moments and the *x* and *z* components for the M1 spins.

structure of $MnFe_3O_5$,[12] but with spins in the *b*-direction, whereas those for $CoFe_3O_5$ are in the *a*-direction. The strong electronic anisotropy of $Co^{2+}$ is likely to be responsible for the latter difference.

## CONCLUSION

The above results demonstrate that the series of orthorhombic $Sr_2Tl_2O_5$-type $MFe_3O_5$ ferrites can be extended to M = Co, although a Co-deficient $Co_{0.6}Fe_{3.4}O_5$ phase was obtained from synthesis at 12 GPa, suggesting that higher pressures may be required to stabilize the ideal stoichiometry.

The cation distribution determined from neutron diffraction is found to be profoundly different from those in previously studied $MFe_3O_5$ derivatives of $Fe_4O_5$. Materials with $M^{2+}$ = Ca and Mn cations larger than $Fe^{2+}$ adopt normal cation distributions with $M^{2+}$ only at the trigonal prismatic sites. The present study shows that $Co^{2+}$ substitutes more evenly across trigonal prismatic and octahedral sites, so the cation distribution lies between normal and inverse $MFe_3O_5$ limits. A surprisingly strong preference for Co to substitute at just one of the two octahedral sites is also revealed. This likely reflects differing site potentials, although the disorder within our sample does not lead to a significant difference between octahedral site bond valence sums.

$CoFe_3O_5$ shows complex magnetic behavior with weak ferromagnetism (canted antiferromagnetism) below $T_{C1} \approx 300$ K and a second transition to ferrimagnetic order at $T_{C2} \approx 100$ K. Spin scattering of carriers leads a substantial increase in the hopping activation energy below $T_{C1}$, and a small negative magnetoresistance is observed at low temperatures.

## ■ ASSOCIATED CONTENT

### Ⓢ Supporting Information

The Supporting Information is available free of charge on the ACS Publications website at DOI: 10.1021/acs.inorgchem.8b02458.

Additional data and experimental details (PDF)

### Accession Codes

CCDC 1866328−1866335 contain the supplementary crystallographic data for this paper. These data can be obtained free of charge via www.ccdc.cam.ac.uk/data_request/cif, or by emailing data_request@ccdc.cam.ac.uk, or by contacting The Cambridge Crystallographic Data Centre, 12 Union Road, Cambridge CB2 1EZ, UK; fax: +44 1223 336033.

## ■ AUTHOR INFORMATION

### Corresponding Author

*E-mail: j.p.attfield@ed.ac.uk.

### ORCID

J. Paul Attfield: 0000-0001-9763-3987

### Funding

We acknowledge financial support from European Research Council (ERC) and Engineering and Physical Sciences Research Council (EPSRC) UK.

### Notes

The authors declare no competing financial interest.

Data that support the findings of this study have been deposited at https://datashare.is.ed.ac.uk/handle/10283/838.

## ■ ACKNOWLEDGMENTS

We acknowledge Science and Technology Facilities Council (STFC) UK and the ESRF for provision of beamtime. We would also like to thank Pascal Manuel (ISIS) and Angel M. Arevalo-Lopez, Paul M. Sarte, Alexander J. Browne, Giuditta Perversi, and James Cumby (Edinburgh) for assistance provided.

## ■ REFERENCES

(1) Verwey, E. J. W. Electronic conduction of magnetite (Fe3O4) and its transition point at low temperatures. *Nature* **1939**, *144*, 327−328.

(2) Senn, M. S.; Wright, J. P.; Attfield, J. P. Charge order and three-site distortions in the Verwey structure of magnetite. *Nature* **2012**, *481*, 173−176.

(3) Lavina, B.; Dera, P.; Kim, E.; Meng, Y.; Downs, R. T.; Weck, P. F.; Sutton, S. R.; Zhao, Y. Discovery of the recoverable high-pressure iron oxide Fe4O5. *Proc. Natl. Acad. Sci. U. S. A.* **2011**, *108*, 17281−5.

(4) Ovsyannikov, S. V.; Bykov, M.; Bykova, E.; Kozlenko, D. P.; Tsirlin, A. A.; Karkin, A. E.; Shchennikov, V. V.; Kichanov, S. E.; Gou, H.; Abakumov, A. M.; Egoavil, R.; Verbeeck, J.; McCammon, C.; Dyadkin, V.; Chernyshov, D.; van Smaalen, S.; Dubrovinsky, L. S. Charge-ordering transition in iron oxide Fe4O5 involving competing dimer and trimer formation. *Nat. Chem.* **2016**, *8*, 501−508.

(5) Lavina, B.; Meng, Y. Unraveling the complexity of iron oxides at high pressure and temperature: Synthesis of Fe5O6. *Sci. Adv.* **2015**, *1*, e1400260.

(6) Delacotte, C.; Hüe, F.; Bréard, Y.; Hébert, S.; Pérez, O.; Caignaert, V.; Greneche, J. M.; Pelloquin, D. Structural Transition at 360 K in the CaFe5O7 Ferrite: Toward a New Charge Ordering Distribution. *Inorg. Chem.* **2014**, *53*, 10171−10177.

(7) Delacotte, C.; Bréard, Y.; Caignaert, V.; Hardy, V.; Greneche, J. M.; Hébert, S.; Suard, E.; Pelloquin, D. Transmission Electron Microscopy Study of CaFe5O7: Evidence of a Monoclinic Superstructure at Room Temperature. *Key Eng. Mater.* **2014**, *617*, 237−240.

(8) Delacotte, C.; Bréard, Y.; Caignaert, V.; Hardy, V.; Greneche, J. M.; Hébert, S.; Suard, E.; Pelloquin, D. Morin-like spin canting in the magnetic CaFe5O7 ferrite: A combined neutron and Mössbauer study. *J. Solid State Chem.* **2017**, *247*, 13−19.

(9) Evrard, O.; Malaman, B.; Jeannot, F.; et al. Mise en évidence de CaFe4O6 et détermination des structures cristallines des ferrites de calcium CaFe2+*n*O4+*n* (*n* = 1, 2, 3): nouvel exemple d'intercroissanc. *J. Solid State Chem.* **1980**, *35*, 112−119.

(10) Hong, K. H.; Arevalo-Lopez, A. M.; Cumby, J.; Ritter, C.; Attfield, J. P. Long range electronic phase separation in CaFe3O5. *Nat. Commun.* **2018**, *9*, 2975.

(11) Hong, K. H.; McNally, G. M.; Coduri, M.; Attfield, J. P. Synthesis, crystal structure, and magnetic properties of MnFe3O5. *Z. Anorg. Allg. Chem.* **2016**, *642*, 1355−1358.

(12) Hong, K. H.; Arevalo-Lopez, A. M.; Coduri, M.; McNally, G. M.; Attfield, J. P. Cation, magnetic, and charge ordering in MnFe3O5. *J. Mater. Chem. C* **2018**, *6*, 3271−3275.

(13) Uenver-Thiele, L.; Woodland, A. B.; Miyajima, N.; Ballaran, T. B.; Frost, D. J. Behaviour of Fe4O5−Mg2Fe2O5 solid solutions and their relation to coexisting Mg−Fe silicates and oxide phases. *Contrib. Mineral. Petrol.* **2018**, *173*, 1−16.

(14) Berastegui, P.; Eriksson, S.; Hull, S.; García García, F. J.; Eriksen, J. Synthesis and crystal structure of the alkaline-earth thallates $M_nTl_2O_{3+n}$ (M = Ca, Sr). *Solid State Sci.* **2004**, *6*, 433−441.

(15) Rodriguez-Carvajal, J. Recent advances in magnetic structure determination by neutron powder diffraction. *Phys. B* **1993**, *192*, 55−69.

(16) Larson, A. C.; Von Dreele, R. B. General Structure Analysis System (GSAS). *Los Alamos National Laboratory Report LAUR 86-748*; Los Alamos National Laboratory: Los Alamos, NM, 2004.

(17) Momma, K.; Izumi, F. VESTA 3 for three-dimensional visualization of crystal, volumetric and morphology data. *J. Appl. Crystallogr.* **2011**, *44*, 1272−1276.

(18) Attfield, J. P. Charge ordering in transition metal oxides. *Solid State Sci.* **2006**, *8*, 861−867.

(19) Brown, I. D. VALENCE: a program for calculating bond valences. *J. Appl. Crystallogr.* **1996**, *29*, 479−480.